

---

## **Geospatial Assessment of Urban Heat Island in Port Harcourt L.G.A, Rivers State, Nigeria**

Benita Chidinma Nnah<sup>a\*</sup>, Anthony Ifeanyi Okenwa<sup>b</sup>, Adamson Opeyemi  
Oloyede<sup>b</sup>, Obiora Nwaibe<sup>b</sup>, Alexander Uchenna Agbu<sup>b</sup>

<sup>a</sup>*Department of Geography and Meteorology, Nnamdi Azikiwe University, Awka, Anambra, Nigeria*

<sup>b</sup>*Advanced Space Technology Applications Laboratory, Uyo, Akwa Ibom, Nigeria*

<sup>c</sup>*University of Uyo, Uyo, Akwa Ibom, Nigeria*

<sup>d,e</sup>*National Space Research and Development Agency, Nigeria*

<sup>a</sup>*Email: benny4nma@gmail.com, <sup>b</sup>Email: happytony85@yahoo.com, <sup>b</sup>Email: adamskrd@gmail.com, <sup>b</sup>Email: obiora.nwaibe@yahoo.com, <sup>b</sup>Email: agbualexuche@gmail.com*

### **Abstract**

Urban development comes with its inherent challenges such as ecosystem alteration. Remote Sensing and GIS was used to assess the spatiotemporal variation of the surface urban heat intensity in Port Harcourt, Rivers State, from 1986 to 2018. The study period was chosen with specific objectives to examine land use land cover changes and assess the spatial and temporal extent of the land surface temperature (LST), determine a relationship between LULC and LST and examine the urban heat island (UHI) intensity using the Getis-Ord Hotspot Analysis. Landsat TM, ETM+ and OLI images of the study area (1986, 2003 and 2018) were implemented to carry out the study. The results of the land use and land cover analysis revealed that urbanised areas increased and covered 51% of the study area from 1986 to 2018. Vegetative cover reduced drastically between this time period, from 57% in 1986 to 30% in 2018, as forested regions made way for urban development to occur. Bare surfaces reduced in spatial extent over the study period, while water bodies within the study area increased. The results of the land surface temperature revealed that surface temperature increased consistently between 1986 and 2018, which was a direct consequence of the increasing urban areas.

---

\* Corresponding author.

In 1986 the average temperature over the study area was estimated at 20.6°C in 1986 to 27.1°C in 2003, increasing to 33.2°C by 2018. The results showed that there is a relationship between urban land and land surface temperature indicated a strong relationship between the two variables, as surfaces with impervious materials were associated with the highest LST values. The number of hotspots within the study area were found to be increasing in number and intensity over the years, with the most concentrations of hot spots found in the northern and central parts of the study area.

**Keywords:** Land use change; Remote sensing; land surface temperature; urban heat island.

## **1. Introduction**

It has been anticipated that cities will accommodate up to 70% of the global population by 2050 according to the report of Department of Economic and Social Affairs in 2012. Compared to the current urbanization rate of 50%, almost all the expected global population growth will be accommodated in cities. Such a rate of rapid urbanization means higher densities in existing cities and many newer urban areas to accommodate up to 2 billion new urban dwellers. However, the rapid urban development in fast-growing cities has resulted in the cities overlooking the environmental and social aspects of urban life [13]. A considerable amount of natural landscape is transformed into building mass and hard surfaces, creating environmental threats for existing and future cities. With huge demands for natural resources (i.e. energy, food, water and materials) cities are contributing up to 80% of greenhouse gas (GHG) emissions, resulting in global warming. Such an increase in temperature will have a severe impact on natural ecosystems and human life in cities, including public health and the quality of public space. Urban development replaces natural surfaces and vegetation with the dry, hard surfaces and structures of roads, footpaths, and buildings. On sunny days, these surfaces accumulate and store solar heat energy and with the surfaces impervious meaning that when it rains the water drains away rapidly leaving little moisture in the ground layer and consequently reducing cooling via evapotranspiration [1]. In addition to this, sources of heat in the urban environment such as air conditioners and vehicle engines, often lead to warmer air temperatures in urban areas than in the surrounding rural areas. This is particularly noticeable at night when the heat that is stored in the urban landscape is slowly released, increasing the temperature differential between urban and rural areas. This is referred to as the Urban Heat Island effect (UHI), which is generally considered as the measure of the differences in air temperatures between urban and rural areas. Both local and international studies have found that the Urban Heat Island effect can add between 1°C to 6°C to ambient air temperature and is likely to be further exacerbated by climate change [19]. The urban heat island phenomenon leads to a host of problems for city inhabitants. It makes cities less comfortable due to thermal discomfort and the increased temperature can potentially increase ill health as certain bacteria thrive in hot environments. In extreme cases, it can even kill people during heat waves [9]. The heat wave occurrences in major cities has been widely studied and is proven to be a direct consequence of the increased artificial surfaces. They directly contribute to increased mortality rates, as in the United States alone, an average of 1000 people die each year of extreme heat. This is higher than due to all other weather events combined [8]. The use of remotely sensed data has been widely applied as a tool to effectively study the influence of urban LULC dynamics on SUHI across the world [5]. These studies rely on land surface temperatures derived from remotely sensed data as opposed to the traditional methods of measuring the UHI which involved comparison of

temperature data from in-situ urban and non-urban meteorological stations [10] or by collecting temperature data by transecting between an urban and non-urban area [9]. Studies have shown that remotely sensed LST can provide a spatially continuous data over a whole city or region, permitting visualization of spatial relationships between temperature patterns and urban land use including infrastructural features [14]. The Urban Heat Island (UHI) of Lokoja town and surroundings was assessed from LandSat ETM satellite imagery of 2006 using remote sensing techniques [19]. Band 3, 4 and 6 of the imagery were used in the estimation of NDVI, land surface emissivity and surface temperature. The results showed that urban heat island in Lokoja town is significant, with average LST values range from 28.13<sup>0</sup>C to 33.62<sup>0</sup>C, and maximum urban/suburban temperature difference reaching 10.9<sup>0</sup>C. His results suggested that vegetation is the principal determinant controlling the spatial distribution of land surface heat flux. This approach was found to be more effective in assessing urban heat island than using the conventional “in situ” temperature estimation. The characteristics of urban heat island (UHI) effect and its causes was analysed by using MODIS data in April 2007 [22]. Surface parameters from the MODIS data have surface temperature (ts), albedo( $\alpha$ ), and normalized difference vegetation index (NDVI). This study first identified patterns of land cover changes between the periods and investigated their impacts on LST, then applied artificial neural network to simulate land cover changes for 2019 and 2029; and finally, estimated their impacts on LST in respective periods. This study is designed as an experimental research. The research is a satellite based assessment of the intensity of the surface urban heat island of Port Harcourt, with land surface temperature datasets the main population of the study. The analysis of the urban heat intensity will involve the analysis of the difference between rural and urban areas in Port Harcourt metropolis.

## **2. Study area**

The study area is located in the southern part of Nigeria. Port-Harcourt L.G.A of River state in Nigeria is positioned between Latitudes 4° 45' N, and 4° 55' N and Longitudes 6° 55' E and 7° 05' E (See Fig. 1). Port-Harcourt is located at about 25 km from the Atlantic Ocean and it is situated between the Dockyard Creek/Bonny River and the Amadi Creek [15,16]. The study area has a mean annual rainfall about 2,000mm [4]. Port-Harcourt has an average monthly temperature above 27°C and there is adequate moisture in virtually all the months. In the city, temperatures are relatively constant (high with a mean maximum of about 34°C and a mean minimum of about 21°C); showing little variation throughout the course of the year [12]. The relief of the study area is low-lying, and the rivers are influenced by tidal fluctuation. Port Harcourt lies at an average altitude of about 12m above mean sea level. In terms of general surface features, Port Harcourt is very unique. The area falls within the coastal belt dominated by Low-Lying coastal plains which structurally belong to the sedimentary formation of the recent Niger Delta [21]. The vegetation of Port Harcourt is made up of equatorial rainforest. The vegetation could be subdivided into two major groups; the tropical rainforest and swamp forest (which is further sub-divided into fresh and mangrove swamps). However, the tropical forest and swamp forest characteristics have been lost to continuous agriculture and urbanization in such a way that the few patches that remain are found in shrines.

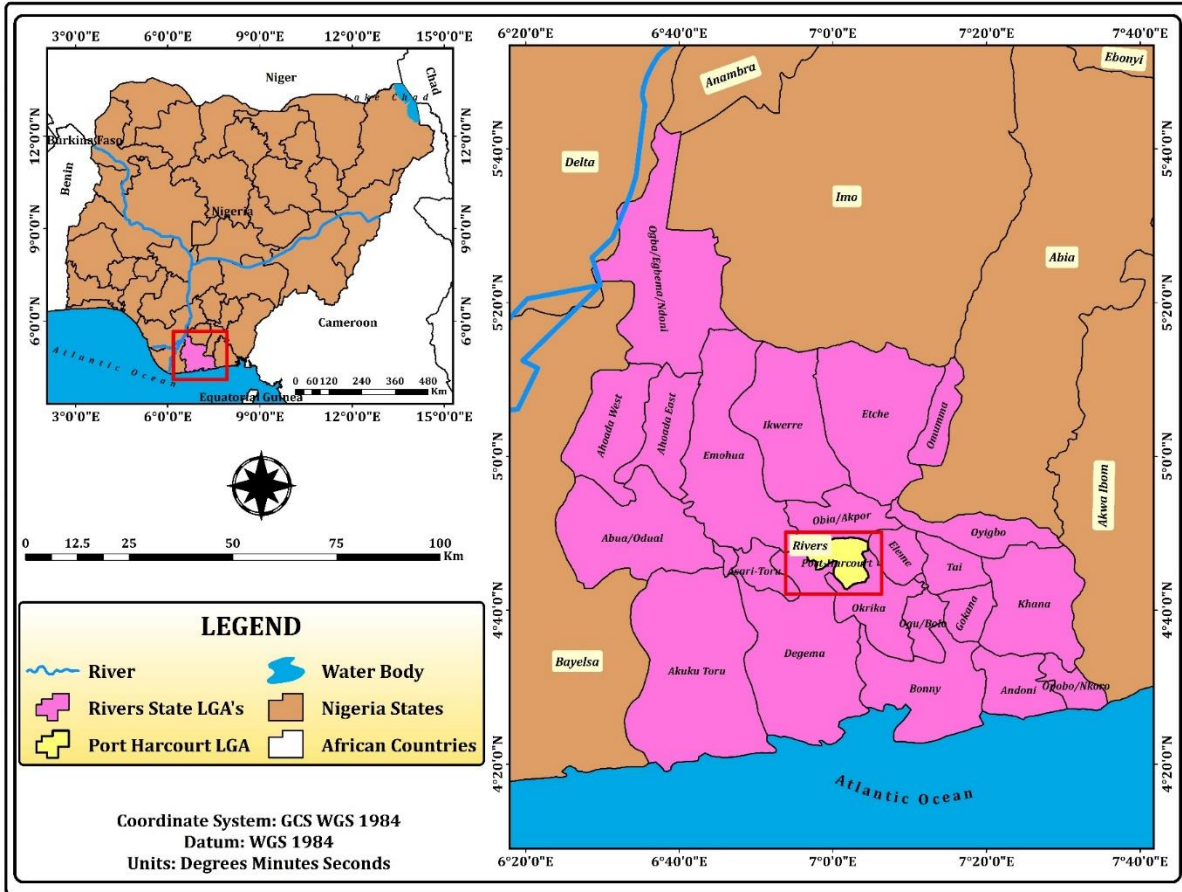


Figure 1: Map of study area

### 3. Data and software used

Topographic maps had been used to extract info-layers such as the administrative boundaries. The LANDSAT data were downloaded from USGS Earth Explorer. The Thematic Mapper (TM) image was downloaded for 26<sup>th</sup> Dec., 1986. The Enhance Thematic Mapper plus (ETM+) image was downloaded for 12<sup>th</sup> Dec., 2003 and the Operational Land Imager (OLI) for 28<sup>th</sup> Dec., 2018. The intervals of  $\pm 16$  years was deliberately chosen by the researcher to ensure uniformity between the datasets. The Landsat satellite data have 30m spatial resolutions, and the TM and ETM+ images have spectral range of 0.45-2.35 micrometer ( $\mu\text{m}$ ) with bands 1 to 7 and 8 respectively, while the Operational Land Imager (OLI) extends to band 12. They were used for the image classification and LST extraction. ArcGIS 10.4 software was used for processing and analysis.

### 4. Methodology

This section explains the processes required to achieve the results of the analyses. The analyses carried out are image classification, LST retrieval and the UHI assessment.

#### 4.1 Image Classification

The LANDSAT data were captured under clear conditions (0% cloud coverage for all the images), hence

uniform atmospheric conditions within the images were assumed and no atmospheric corrections were applied. All the images were pre-processed by the USGS to rectify any geometric or radiometric distortions of the image. This correction process employs both Digital Elevation Models and Ground Control Points to achieve a product that is free from distortions related to the Earth (e.g. curvature, rotation), satellite (e.g. attitude deviations from nominal), and sensor (e.g. view angle effects). The USGS also geometrically corrected and georeferenced both images to the WGS1984 datum and Universal Transverse Mercator (UTM) zone 32N coordinate system. For the Landsat TM, ETM+ and OLI, a False Colour Composite (FCC) operation was performed using the ArcGIS 10.4 software and the images were combined in the order of band 5, 4 and 3 for Landsat TM and ETM+ while that of Landsat OLI was in the order of band 6, 5 and 3 due to change in sensor. The images were then clipped to the boundary of Port Harcourt to allow for accuracy. A supervised classification scheme with the Interactive Selection algorithm was used for the classification. The supervised classification was performed by creating a training sample, and based on spectral signature curve, various land-use classes were created namely: Water body, Urban Area, Bare Surface, Vegetative Cover. These classes were observed distinctively on the clipped image and were used for the classification.

#### **4.2 Land Surface Temperature (LST) Estimation**

The mono-window algorithm method is adopted to retrieve the LST from the imageries selected for this study. The Landsat-5 TM thermal band 6 (10.40-12.50  $\mu\text{m}$ ), ETM+ band 6L (10.4 – 12.5  $\mu\text{m}$ ) and TIRS 10 and 11 (10.60 -11.19  $\mu\text{m}$ ) have a spatial resolution of 30m respectively which is considered suitable as shown by many literatures for capturing the multifaceted intra-urban temperature differences thus making it effective for urban climate analysis. For the Landsat ETM+ sensor, images in the thermal band are taken twice: one in the low-gain mode (band 6L) and the other in the high-gain mode (band 6H). Band 6L is used to image surfaces with high brightness, whereas band 6H is for low brightness. Band 6L was used in this study, due to errors contained in the 6H band. Consequently, the LANDSAT thermal bands were used to retrieve LST over the study area for the three different periods (1986, 2003, and 2018) based on the following steps:

##### **STEP 1. Conversion of Digital Numbers (DN) of the bands to Spectral Radiance**

The DN of the thermal bands of TM and ETM+ were converted into spectral radiance values for each of the investigated years using the following equation –

$$L_{\lambda} = \left( \frac{L_{MAX} - L_{MIN}}{Q_{CALMAX} - Q_{CALMIN}} \right) \times (DN - 1) + L_{MIN} \quad - \quad - \quad - \quad (6)$$

Where;

$L_{\lambda}$  = The spectral radiance at the sensor's aperture in  $\text{Wm}^{-2} \text{sr}^{-1} \mu\text{m}^{-1}$

$L_{MAX}$  = Spectral radiance scaled to  $Q_{CALMAX}$  in  $\text{Wm}^{-2} \text{sr}^{-1} \mu\text{m}^{-1}$ , available in the metadata.

$L_{MIN}$  = Spectral radiance scaled to  $Q_{CALMIN}$  in  $\text{Wm}^{-2} \text{sr}^{-1} \mu\text{m}^{-1}$ , available in the metadata.

$Q_{CALMAX}$  = Maximum quantized calibrated pixel value (corresponding to  $L_{MAX}$ ) in DN = 255

$Q_{CALMIN}$  = Minimum quantized calibrated pixel value (corresponding to  $L_{MIN}$ ) in DN = 1

DN = Digital Number of the Band

For Landsat 8 with file data on Radiance Multiplier (M) and Radiance Add (B), the thermal infrared (TIR) band was converted into spectral radiance ( $L\lambda$ ) using the equation -

$$L\lambda = M_L Q_{CAL} + A_L \quad (7)$$

Where;

$L\lambda$  = The spectral radiance at the sensor's aperture in  $Wm^{-2} sr^{-1} \mu m^{-1}$

$M_L$  = Band Specific Multiplicative Rescaling factor, gotten from the metadata of the image

$Q_{CAL}$  = Quantized and calibrated standard product pixel values (Digital Number)

$A_L$  = Band Specific Additive Rescaling factor, gotten from the metadata of the image

## STEP 2. Conversion from Spectral Radiance to At-Satellite Brightness Temperature

Spectral radiance values for the bands were then converted to radiant surface temperature under an assumption of uniform emissivity using pre-launch calibration constants for the Landsat ETM+ sensor implemented into this equation;

$$T = \frac{K_2}{\ln\left(\frac{K_1}{L\lambda} + 1\right)} - 273.15 \quad (8)$$

Where;

T = At-satellite brightness temperature in Degrees Celsius

$L\lambda$  = Spectral radiance in  $Wm^{-2} sr^{-1} \mu m^{-1}$  (gotten from equations 6 and 7)

$K_1$  = Band specific thermal conversion constant from the metadata ( $K1\_CONSTANT\_BAND\_X$ , x is the thermal band number)

$K_2$  = Band specific thermal conversion constant from the metadata ( $K2\_CONSTANT\_BAND\_X$ , x is the thermal band number)

-273.15 = Constant for conversion from Kelvin to Degrees Celsius

**STEP 3. Correcting for Land Surface Emissivity (LSE)**

In estimating LSE, Normalized Differential Vegetative Index (NDVI) was utilized for emissivity correction. The temperature values obtained using Equation (8) are referenced to a blackbody. Therefore, corrections for spectral emissivity ( $\epsilon$ ) became necessary according to the nature of land cover. This equation was used;

$$e = 0.004P_v + 0.986 \tag{9}$$

Where,

e = Land Surface Emissivity

0.004 and 0.986 = Constants for emissivity estimation

$P_v$  = Proportion of vegetation given by the equation –

$$P_v = \left( \frac{NDVI - NDVI_{min}}{NDVI_{max} - NDVI_{min}} \right)^2 \tag{10}$$

NDVI = Normalized Differential Vegetation Index for each of the years

The index is defined by equation below -

$$NDVI = \frac{NIR - RED}{NIR + RED} \tag{11}$$

Where NIR and RED are the reflectance in the near-infrared and red portion of the electromagnetic spectrum respectively.

For LANDSAT 5 TM and 7 ETM+,

$$NDVI = \frac{BAND\ 4 - BAND\ 3}{BAND\ 4 + BAND\ 3} \tag{12}$$

Where Band 4 and Band 3 are the reflectance in the near-infrared and red portion of Electromagnetic spectrum of the Thematic Mapper and Enhanced Thematic Mapper plus respectively.

For LANDSAT 8 OLI,

$$NDVI = \frac{BAND\ 5 - BAND\ 4}{BAND\ 5 + BAND\ 4} \tag{13}$$

Where Band 5 and Band 4 are the reflectance bands in the near-infrared and red portion of Electromagnetic spectrum of Operation Land Imager (OLI) sensor of Landsat 8 respectively.

$NDVI_{min}$  = Minimum value of NDVI for that year

NDVI<sub>max</sub> = Maximum value of NDVI for that year

**STEP 4. Estimation of the Land Surface Temperature**

Finally, having corrected the emissivity in equation (9), the LST was estimated using the equation;

$$LST = \frac{B_T}{1+w} \times \frac{B_T}{P} \times \ln(\epsilon) \quad - \quad - \quad - \quad - \quad - \quad - \quad (14)$$

Where.

LST= Land Surface Temperature in Degrees Celsius

B<sub>T</sub> = At-satellite brightness temperature

W = Wavelength of emitted radiance (µm)

$$p = h \times \frac{c}{s} (1.438 \times 10^{-2} m K) = 14380 \quad - \quad - \quad - \quad - \quad - \quad (15)$$

H = Planck’s constant (6.626 × 10<sup>-34</sup>J/s)

S = Boltzmann constant (1.38 × 10<sup>-23</sup>J/K)

C = Velocity of light (2.998 × 10<sup>8</sup>m/s)

e = LSE

**4.3 Urban Heat Island (UHI) Assessment using Hotspot Analysis**

Hot spot analysis has been achieved by calculating the Getis-Ord statistic for surface temperature in context with neighbouring cell temperatures. The value is an z-score and shows where characteristics with high or low values are clustered. This is carried out with the Hot Spot Analysis (Getis-Ord) tool under Mapping Clusters in the Spatial Analyst toolbox in ArcGIS. The Getis-Ord statistics are calculated according to the formula (ESRI, 2018):

$$G_i^* = \frac{\sum_{j=1}^n w_{i,j} x_j - \bar{X} \sum_{j=1}^n w_{i,j}}{S \sqrt{\frac{[n \sum_{j=1}^n w_{i,j}^2 - (\sum_{j=1}^n w_{i,j})^2]}{n-1}}} \quad - \quad - \quad - \quad - \quad (16)$$

$$\bar{X} = \frac{\sum_{j=1}^n x_j}{n} \quad - \quad - \quad - \quad - \quad (17) \quad (3)$$

$$S = \sqrt{\frac{\sum_{j=1}^n x_j^2}{n} - (\bar{X})^2} \quad - \quad - \quad - \quad - \quad (4) \quad (18)$$

Where,

$G_i^*$  = Resultant G statistics (z-scores and p-values) for pixel i

$x_j$  = LST value for pixel j

$w_{i,j}$  = Spatial weight between pixel i and neighbouring pixel j

n = Total number of pixels

$\bar{X}$  = Mean LST of all pixels

S = Variance

The output of the  $G_i^*$  statistic (the z-score) represents the statistical significance of clustering for a specified distance, which will then be compared with the range of values from the classification table (Table 3.3) to analyse the “very cold spot” and “very hot spot” in order to determine the areas with extreme values.

**Table 3.3:** Classification based on p-value and z-score (Source: Grigoras, 2018)

Significance Level (p Value)	Critical Value (z Score)	Class No.	Class name
-0.01	<-2.58	1	Very cold spot
-0.05	-2.58--1.96	2	Cold spot
-0.10	-1.96--1.65	3	Cool Spot
0	-1.65-1.65	4	Not significant
0.10	1.65-1.96	5	Warm spot
0.05	1.96-2.58	6	Hot spot
0.01	> 2.98	7	Very hot spot

Points from the hotspot analysis were generated, and the temperature readings for each hot or cold spot will be extracted using the “Extract Multi Values to Point” tool in ArcGIS 10.4. Then, the urban heat island will be assessed using the equation;

$$UHI = T_H - T_C \quad \text{---} \quad (19)$$

Where;

UHI = Urban Heat Intensity

$T_H$  = Temperature at hot spot (representing the urban region)

$T_C$  = Temperature at cold spot (representing the rural region)

**5. Results and Discussion**

The land cover for each representative year per interval was classed into 5 classes – Water body, Urban Area, Bare Surface and Vegetative Cover. These classes were assessed for their spatial and temporal variations from 1986 to 2018. The classes were further analyzed to detect the changes that have occurred between them. Figure 2-4 shows the spatial coverage of land use in Port Harcourt in 1986. It is observed here how vast vegetative cover was, given that the population boom experienced in the 21<sup>st</sup> century had not yet occurred in this L.G.A. The urbanized areas were dense in towns like Amatagwolo, Port Harcourt, Diobu etc.

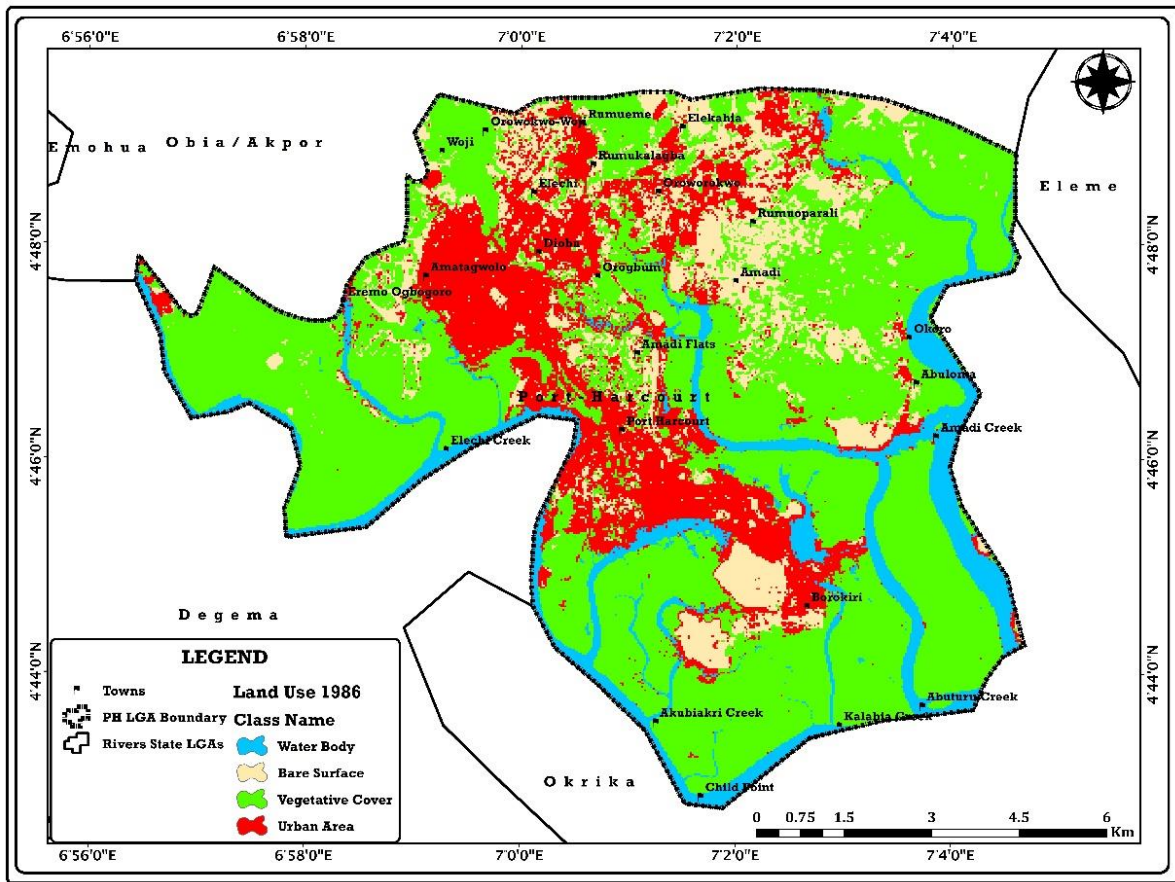


**Figure 5.1:** Land use of Port-Harcourt 1986

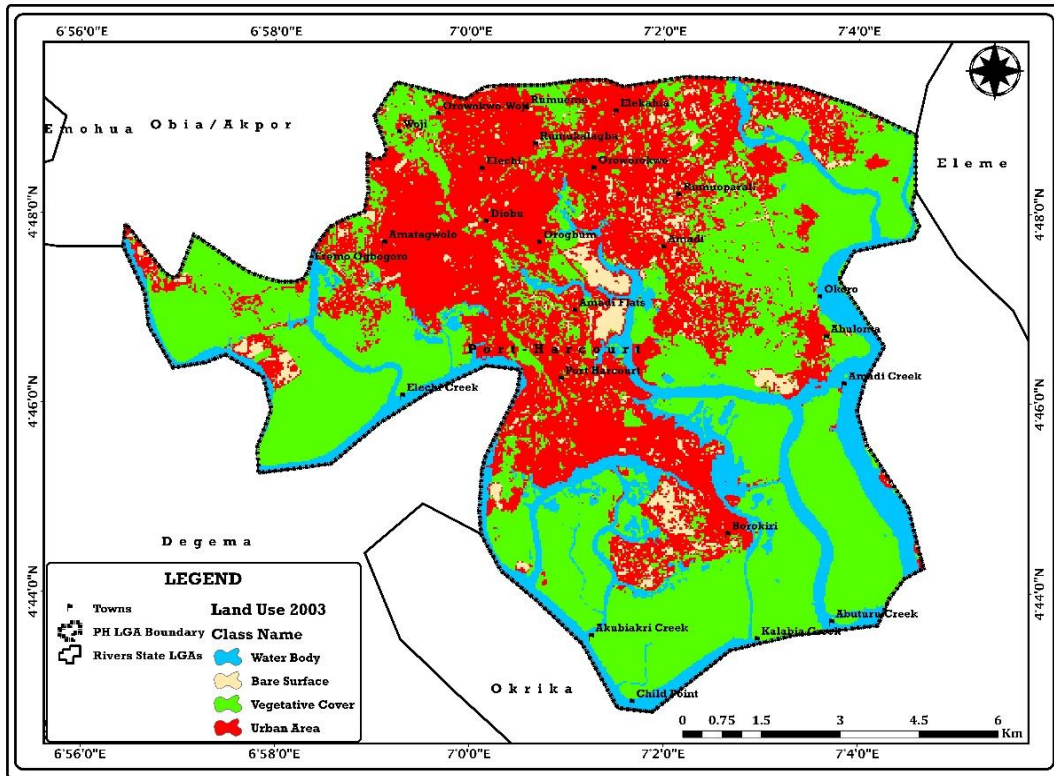


Figure 5.2: Land use of Port-Harcourt 2003

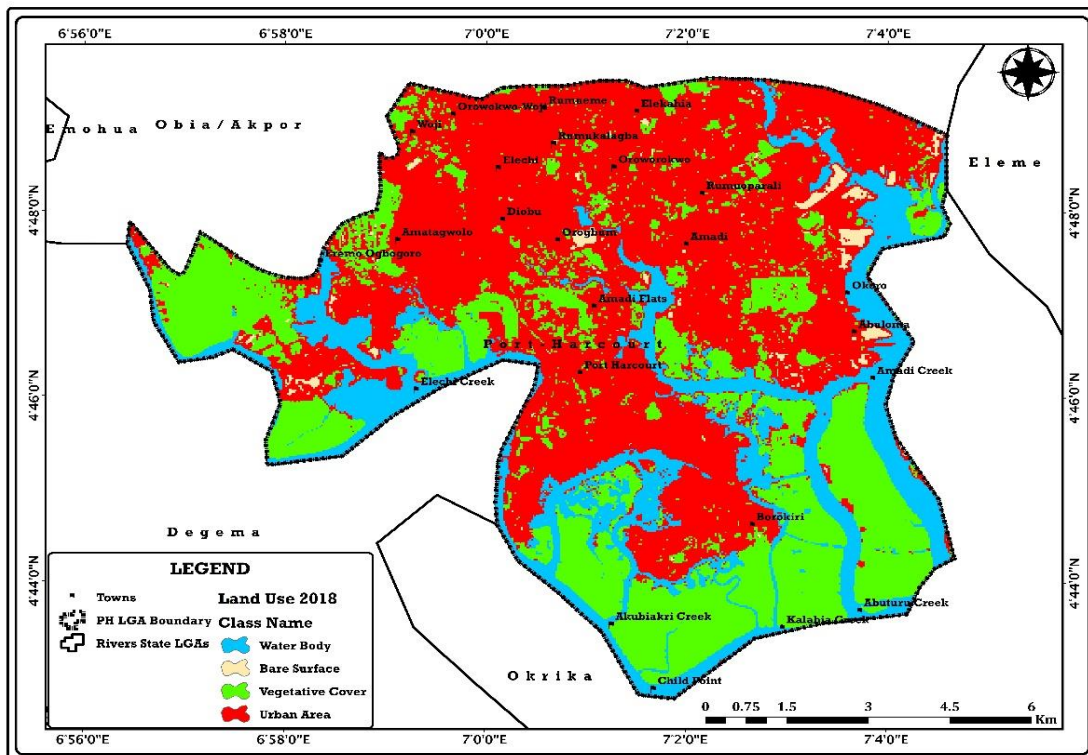
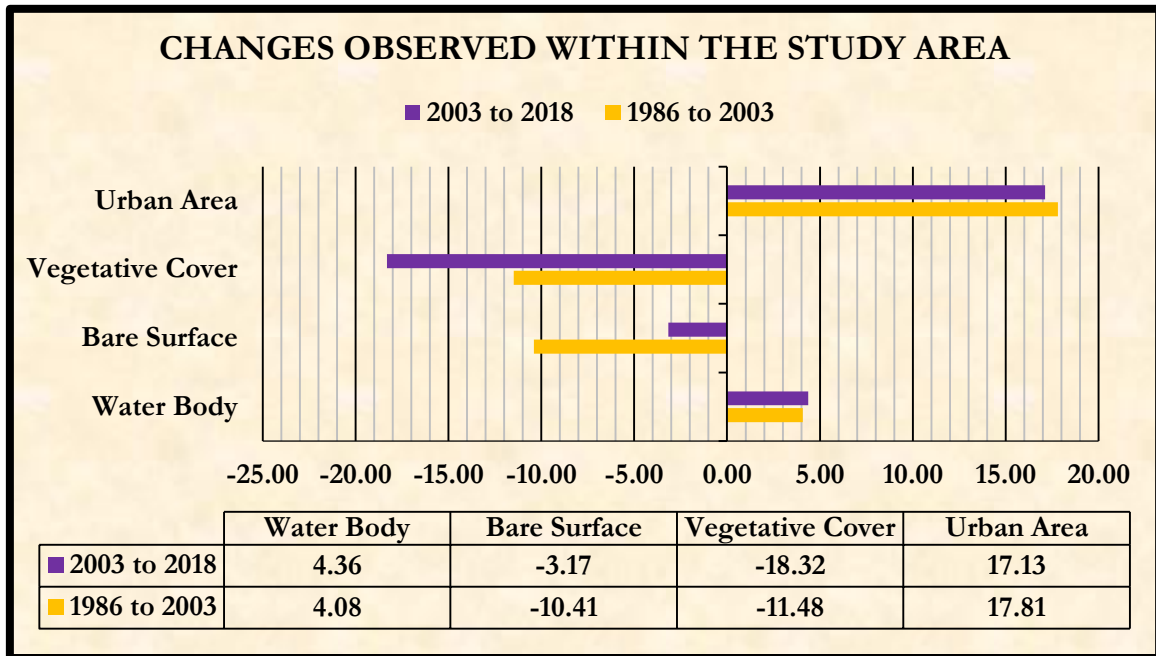


Figure 5.3: Land use of Port-Harcourt 2018

**5.1 Change Detection in Land Use Pattern in PH from 1986 to 2018**

The Land use from 1986 to 2003, urban areas increased significantly by 17.81 km<sup>2</sup>, due to expansion in residential areas coupled with increasing anthropogenic activities over the region resulting from dynamic population growth that occurred between these years (Fig. 5.4).



**Figure 5.4:** Changes observed in land use classes

**5.2 Accuracy Assessment**

It is very important to derive information from remotely sensed data at local, regional, and global scales (Johannsen and his colleagues 2003). The thematic information must be accurate in order to make decision throughout the world (Jensen, 2007). However, errors always occur when we derive the thematic information. As the result, remote sensing thematic maps should be subjected to a thorough accuracy assessment before being used in scientific investigations and policy decisions (Stehman and Czaplewski, 1998). Anderson and his colleagues (1976) determined that the overall accuracy of LULC maps for natural resource management should be above 85% and it must be approximately equal for most categories. The confusion matrix was used to determine the accuracy of the classified images.

From the table above, the overall accuracy for 1986, 2003 and 2018 are 96%, 94% and 96% respectively, while the overall kappa stood at 98%, 95% and 97% respectively. This falls adequately in line with the accuracy limit of 85% posited by Anderson and his colleagues (1976) modified by Eastman (2009). A major inference from these results is that the overall map accuracy of 96.6% was satisfactory for the research considering the fact that Anderson and his colleagues (1976) postulated 85% as essential accuracy minimum for a research of this nature.

**Table 5.1:** Accuracy Assessment Table

LULC classes	Kappa Index of Agreement (KIA)		
	1986	2003	2018
Urban Area	0.9506	0.8856	0.9449
Vegetative Cover	0.9800	0.9300	0.9974
Water Body	1.0000	1.0000	1.0000
Bare Surface	0.8446	0.8361	0.8430
<b>Overall Accuracy</b>	<b>0.961 (96%)</b>	<b>0.9424 (94%)</b>	<b>0.9620 (96%)</b>
<b>Overall Kappa</b>	<b>0.9860 (98%)</b>	<b>0.9501 (95%)</b>	<b>0.9738 (97%)</b>
<b>Total Average Accuracy = 96.6%</b>			

**5.3 Spatial and Temporal Variations in Land Surface Temperature (LST)**

In 1986, the temperature ranged between 16°C and 24.8°C within Port Harcourt (Fig. 5.5.). From the LULC analysis in section 5.0, it was determined that vegetative cover was over 57% of the study area by this time, and when coupled with the low level of urbanisation in this area, the low level of temperature is further acknowledged. The built-up areas in Port Harcourt as of 1986, were likely of lower structural density and hence could absorb radiative solar energy. Also, there were lesser anthropogenic activities going on by then, which had less impact on the range of the LST distribution. The average temperature of the region in 1986 is estimated at 20.6°C.

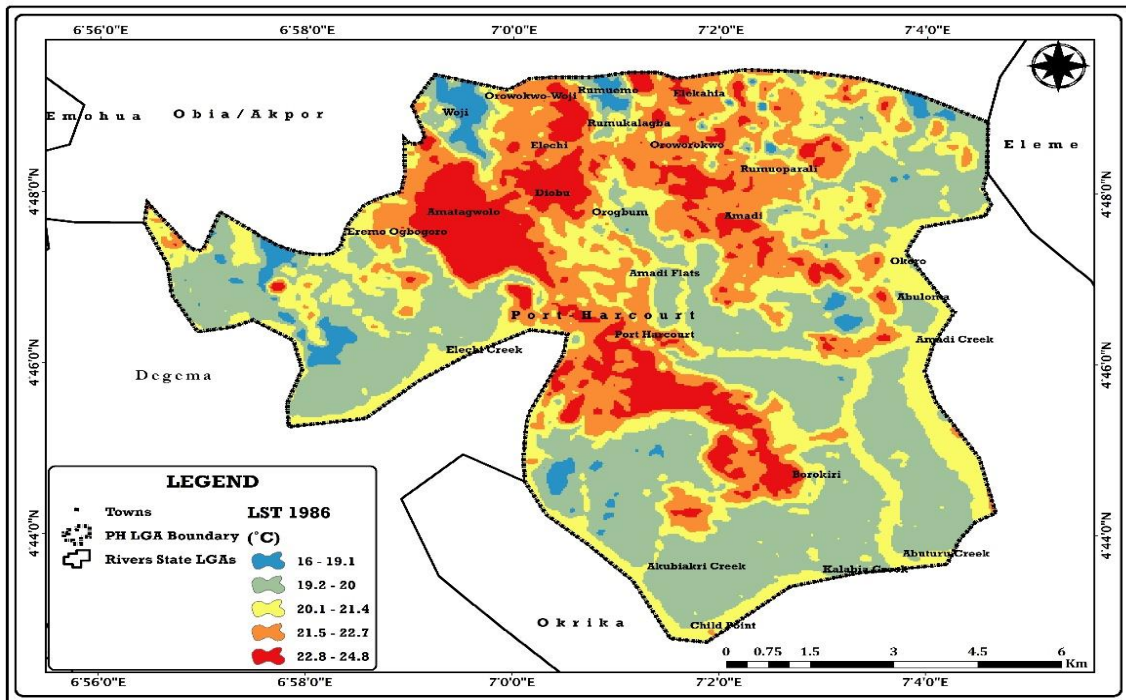


**Figure 5.5:** LST in 1986

By 2003, the temperature values had risen to a minimum of 23.5°C and maximum of 31.9°C (Fig. 5.6), with an average of 27.1°C, an alarming increase in surface temperature. Given that increased anthropogenic activities, higher rural-urban migration, and population increase was observed within this period, the growth of urban impervious surfaces contributed to the increase in temperature recorded. This increase in temperature coincided perfectly with the drastic reduction in vegetative cover over the area. Vegetated areas act as carbon sinks in regions where they are clustered, also creating a cooling atmosphere, absorbing temperatures. In regions where they reduce. These functions are mitigated, and the negative consequences associated with their lack become prevalent. This was the case in Port Harcourt, given that the loss of vegetation and increased built up areas led to an increase in temperature.

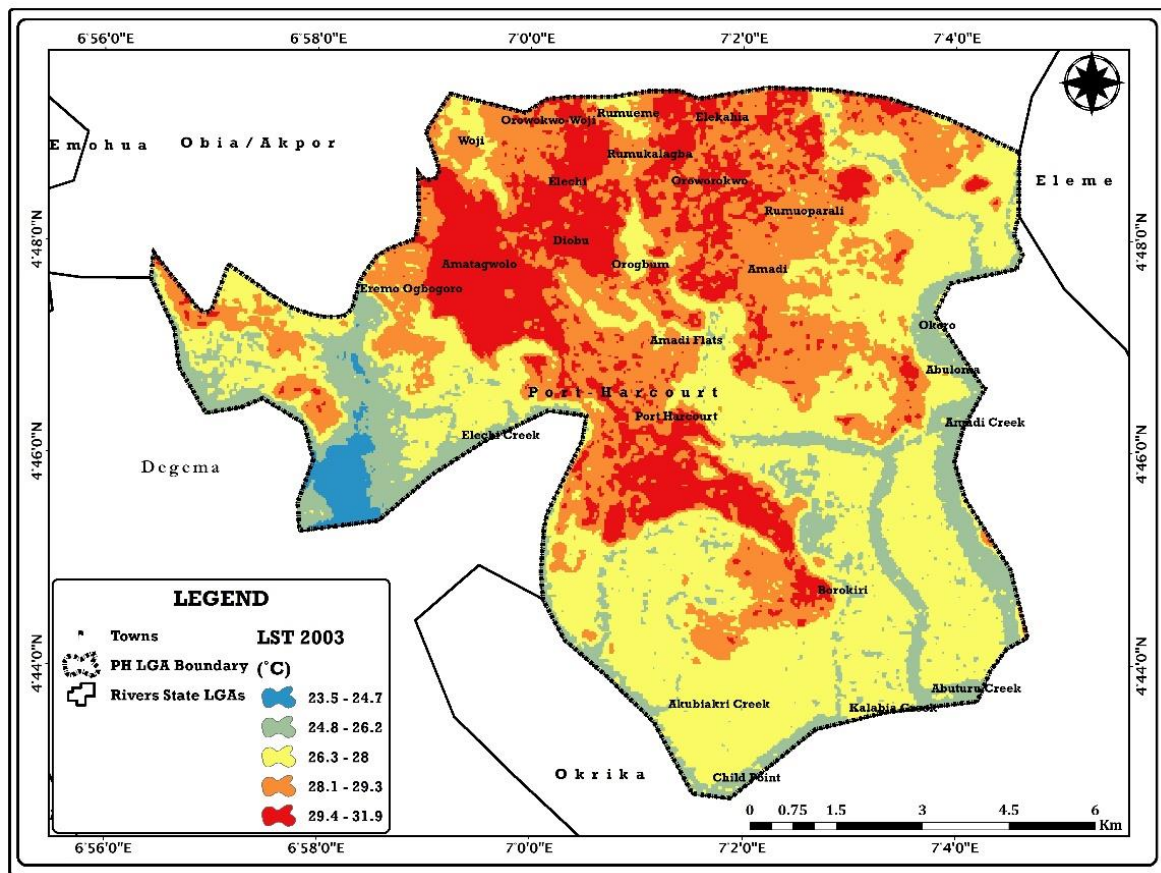


Figure 5.6: LST in 2003

The temperature values increased to a maximum of 38.3°C to 24.3°C in 2018, with an average of 33.2°C observed from the analysis. By this time, vegetated surfaces had reduced to barely 30% of the study area, with urban areas growing to cover 51% of the study area. The growing populations lead to an increase in urban development, with surfaces impervious in nature being used to create buildings, roads and various other infrastructure within the study area. Port Harcourt is a region characterized by high populations, and rapid developments. The increase in anthropogenic activities by the inhabitants of the region creates a greenhouse effect as gases which trap temperatures are released into the atmosphere, and actively increase the temperature levels within the region. The high temperatures observed within Port Harcourt can be attributed to these

occurrences.

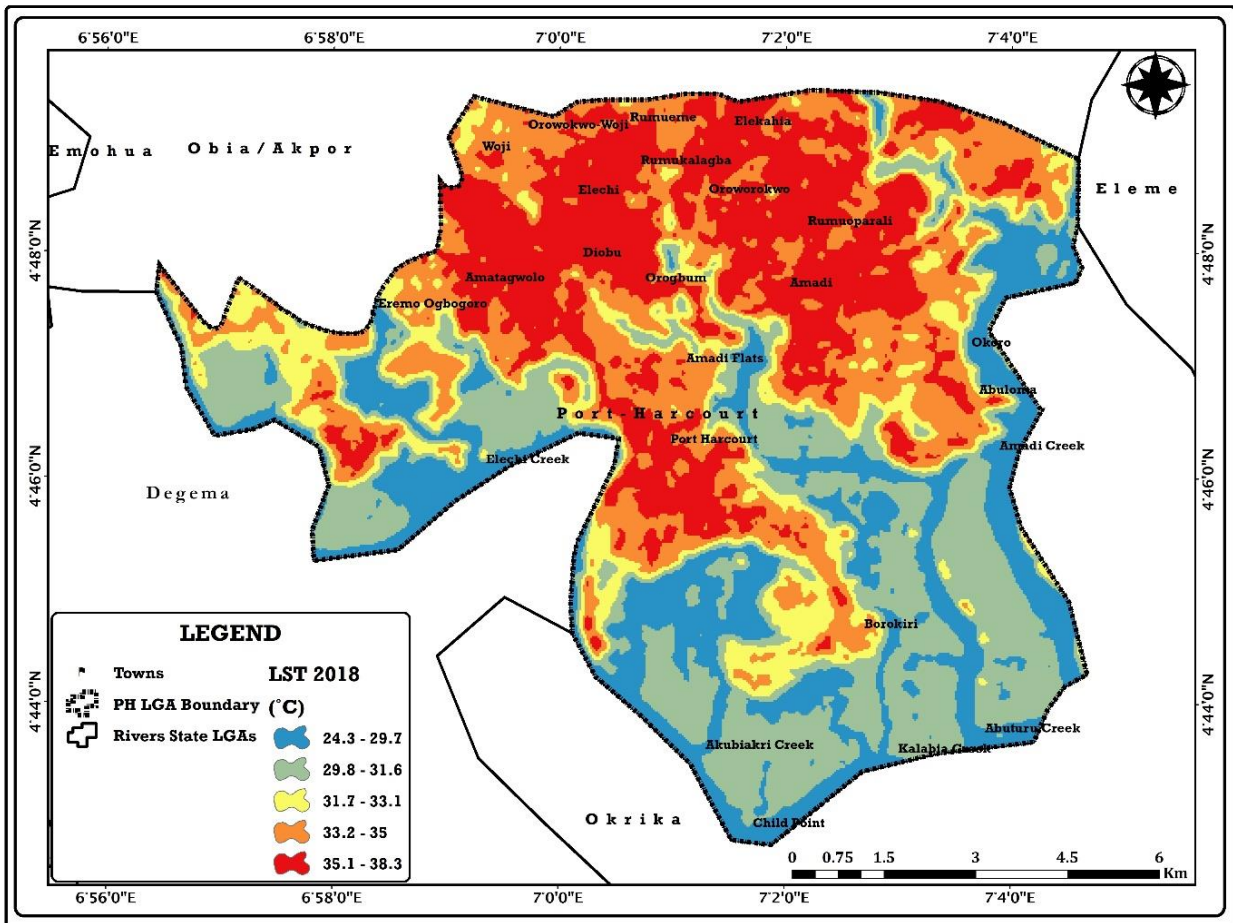
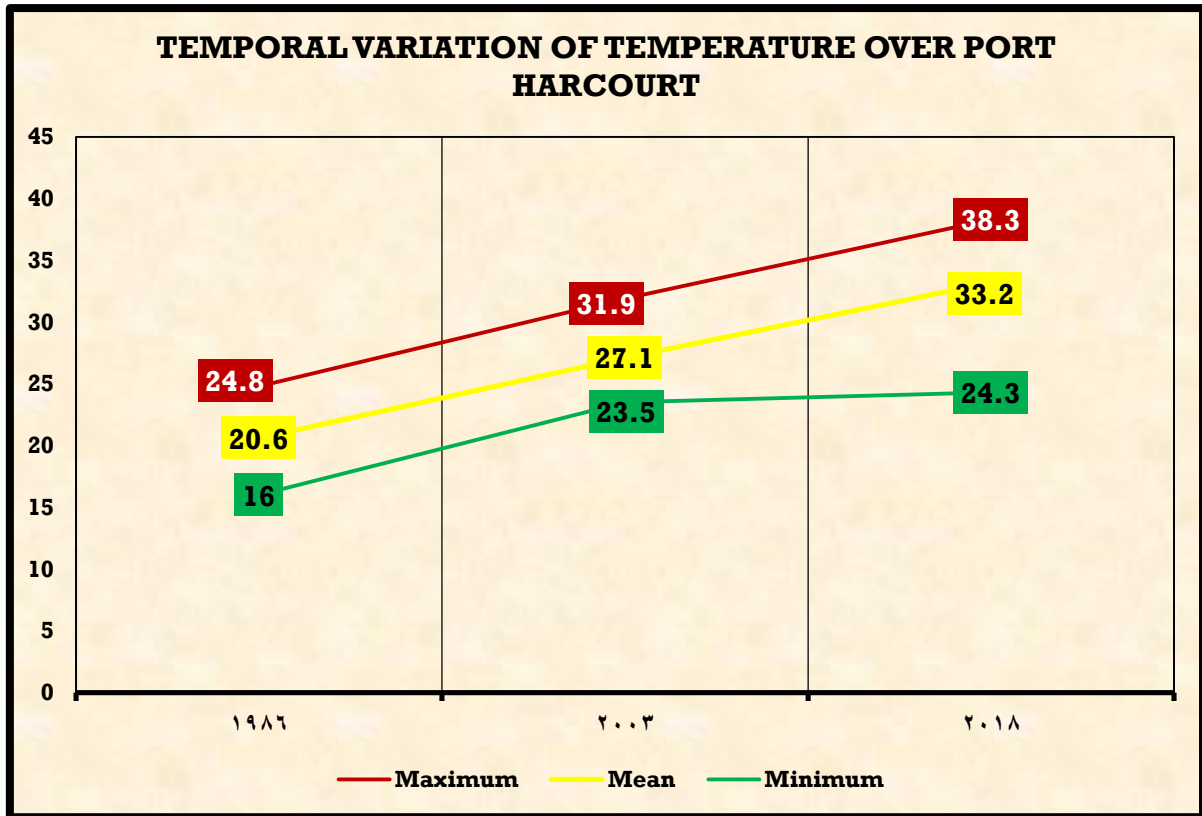


Figure 5.7: LST in 2018

The concurrent increase in temperature is further depicted in Fig. 5.8. The minimum values have been steady increasing, indicating that even water bodies are following the trend of rise in sea temperature observed in the past climatic year by various researches. The values increased from 16°C in 1986 to 23.5°C in 2003, with a slightly higher 24.3°C observed in 2018. This trend occurs in the maximum recorded temperatures within the study area, as it grew from 24.8°C in 1986 to 38.3°C in 2018. The average temperature which gives a clearer assessment of the temperatures observed and their extents, is found to be increasing from 20.6°C in 1986 to 27.1°C in 2003. However, in 2018 the average temperature had grown to 33.2°C, an alarming level of increase. A direct impact of this increase is on the thermal discomfort experienced by inhabitants of the region, coupled with the high risk of a heat wave and increased mortality rates.



**Figure 5.8:** Temporal variation of temperature values over Port Harcourt from 1986 to 2018

When the changes in temperatures between the time periods are keenly assessed, it is observed that the most changes occurred between 1986 and 2003, a change in average temperatures of 6.5°C, whereas that of 2003 to 2018 was found to be 6.1°C. The variations in the maximum and minimum temperature further enhance this difference, as the change in maximum temperatures account for 7.1°C between 1986 and 2003, while between 2003 and 2018 it was 6.4°C. The minimum temperatures stood at a change of 7.5°C between 1986 and 2003, whereas it was a mere 0.8°C between 2003 and 2018.

**5.4 Determination of the Urban Heat Island Intensity using Hotspot Analysis**

The results of hot spot analysis performed using Getis-Ord Gi\* spatial statistics over the study area from 1986 to 2018 are analysed and discussed below. Their presence per period is assessed, and the persistence of each hotspot further determined to depict regions at high risk of high temperatures and associated negative consequences. Between 2003 and 2018, urban areas increased in spatial extent to further handle the excessive populations and provide adequate services. This increase led to the further development of hot spots within the study region, as observed in Fig.5.9. The most substantial development of these hotspots was found to be in the eastern region of the study area, where most not-significant spots were changed to warm, hot and very hot spots. The cold spots gravitated more towards the southern part by 2018, mostly due to the increase in urbanisation occurring up north, and the presence of water bodies.

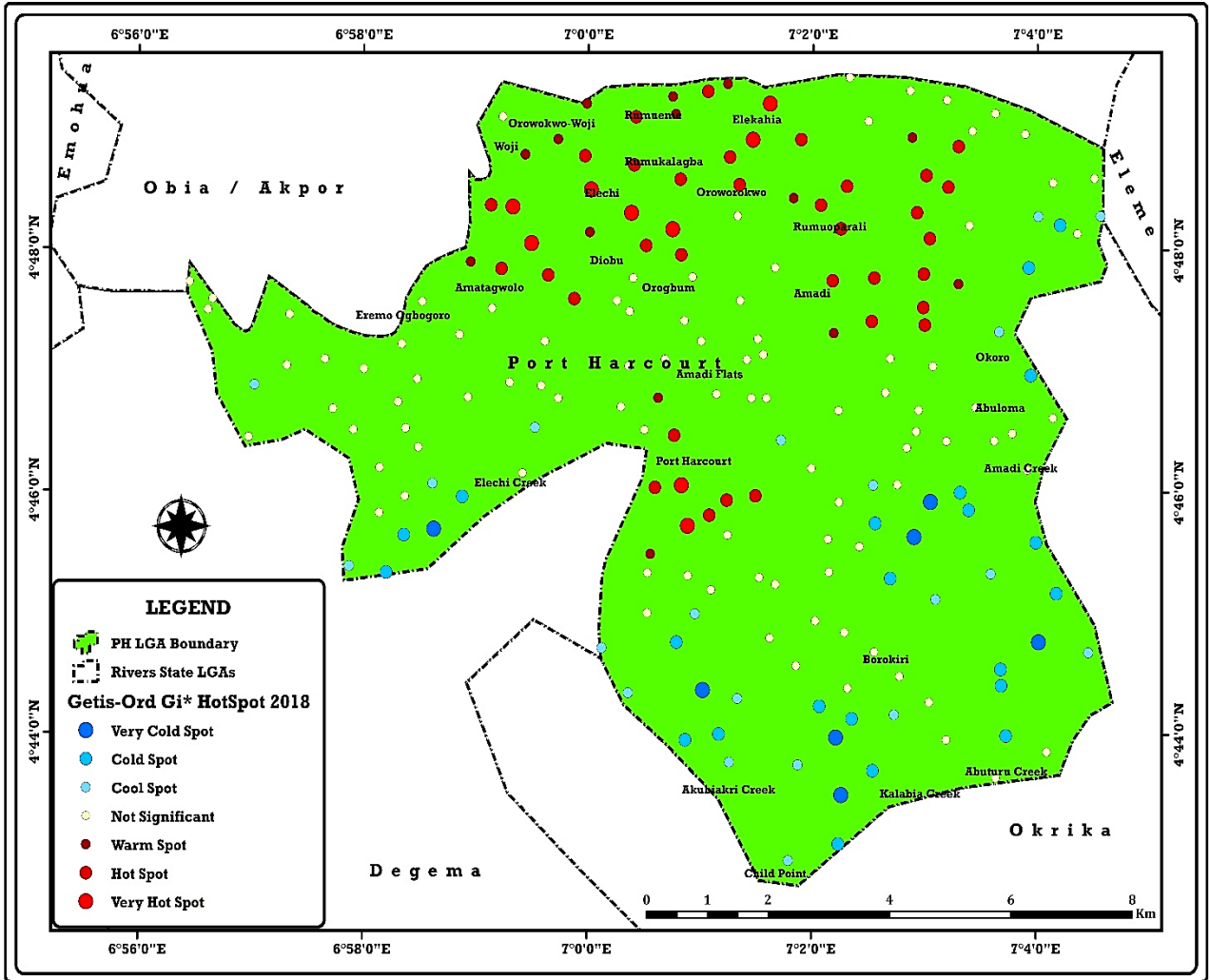


Figure 5.9: Hot and Cold Spots in PH for 2018

#### 5.4.1 Hotspot LST Assessment

The hotspots were utilised in extracting their associated value pixel for Inverse Distance Weighting (IDW) interpolation, to display a rasterised map of the spatial distribution of the LST for the hotspots. This was carried to further determine the adequacy of implementing hotspot analysis in urban heat island studies. Fig. 5.10 below demonstrates the extent of the hot spot land surface temperatures within Port Harcourt in 1986. Amatagwolo, Diobu, Elechi and Port Harcourt were associated with the highest intensities of the LST within the study area by this period. The lowest intensities are recorded at Elechi Creek, Akubiakiri and other creeks further south.

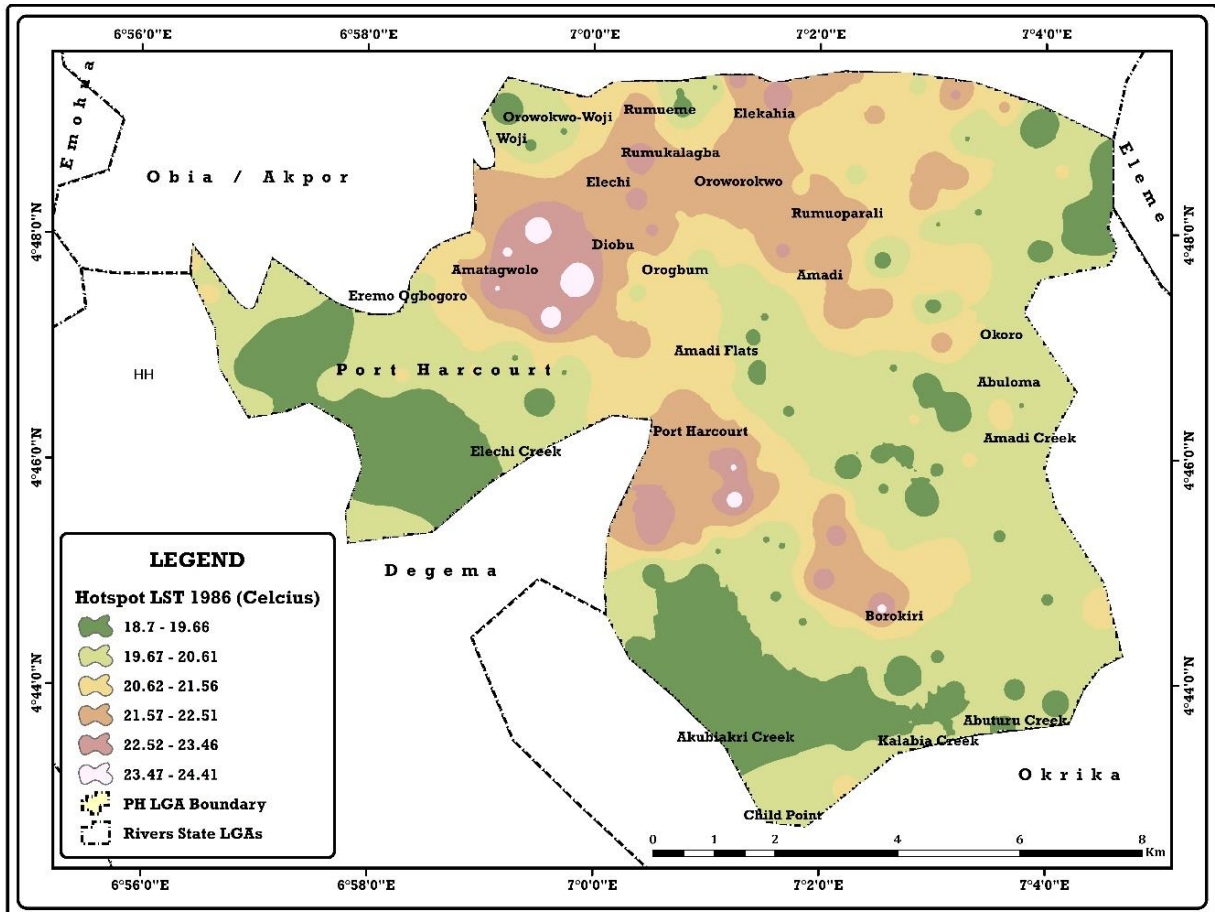


Figure 5.10: LST using Hotspots within Port Harcourt in 1986

By 2003, the spatial extent of the higher intensities increased to a larger percentage of the study area, with towns such as Rumukalagba, Elekahia and Oroworokwo (Fig. 5.11) growing to contribute to the increased LST values. Their urban development within this time is a substantial reason for the increased temperature values, as vegetative cover was replaced with impervious surfaces. The lowest values were found around the western region of the study area.

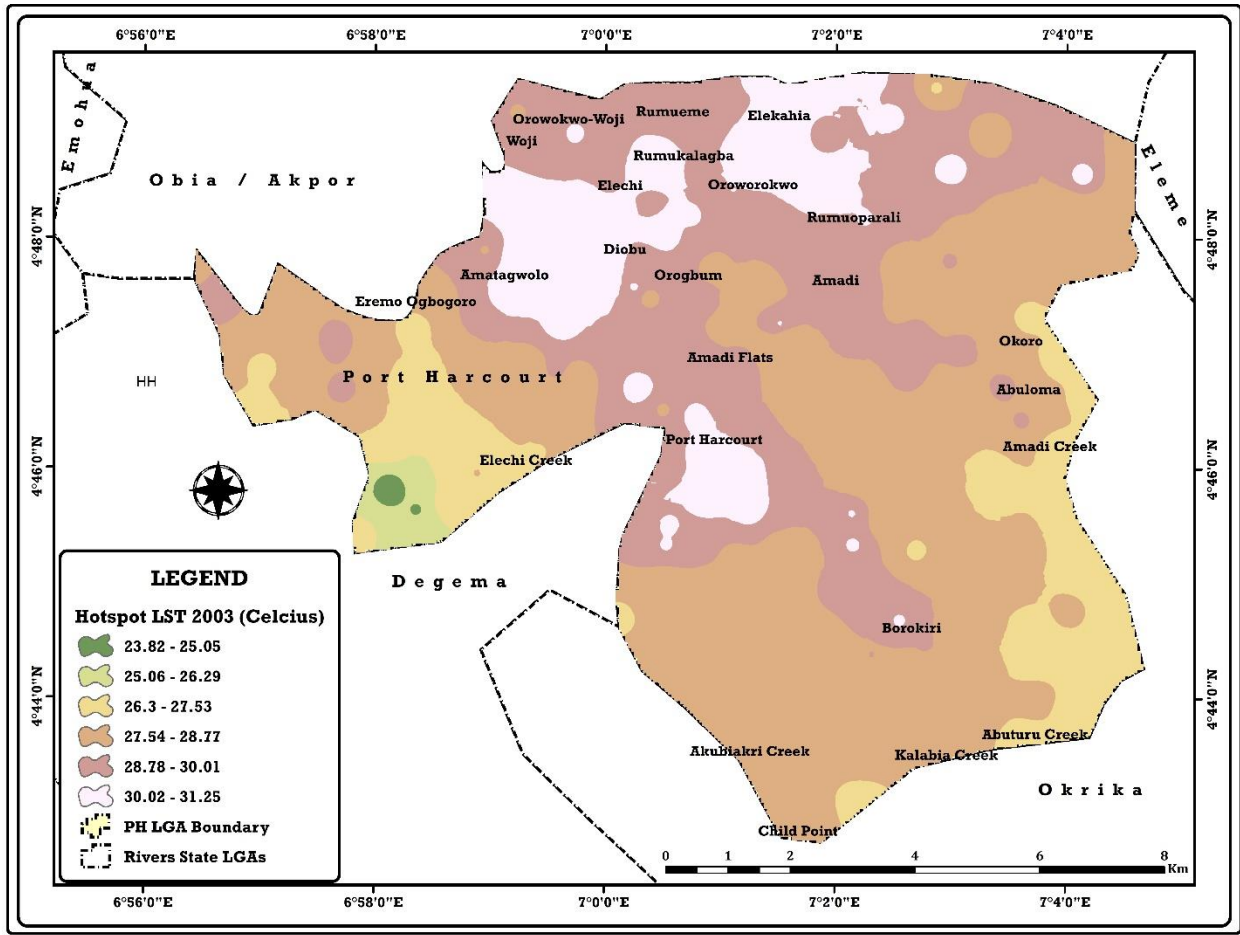


Figure 5.11: LST using Hotspots within Port Harcourt in 2003

By 2018, the LST values further increased to readings of about 37°C in towns such as Woji, Amadi, Rumuokparali amongst others. The increase in surface temperature poses a host of problems from health to economic negative consequences. Amatagwolo, Elekahia, Port Harcourt, Elechi etc experienced rapid development within their localities, which caused the increase in temperature observed within these towns. The lowest values were once more observed near the creeks and water bodies in general.

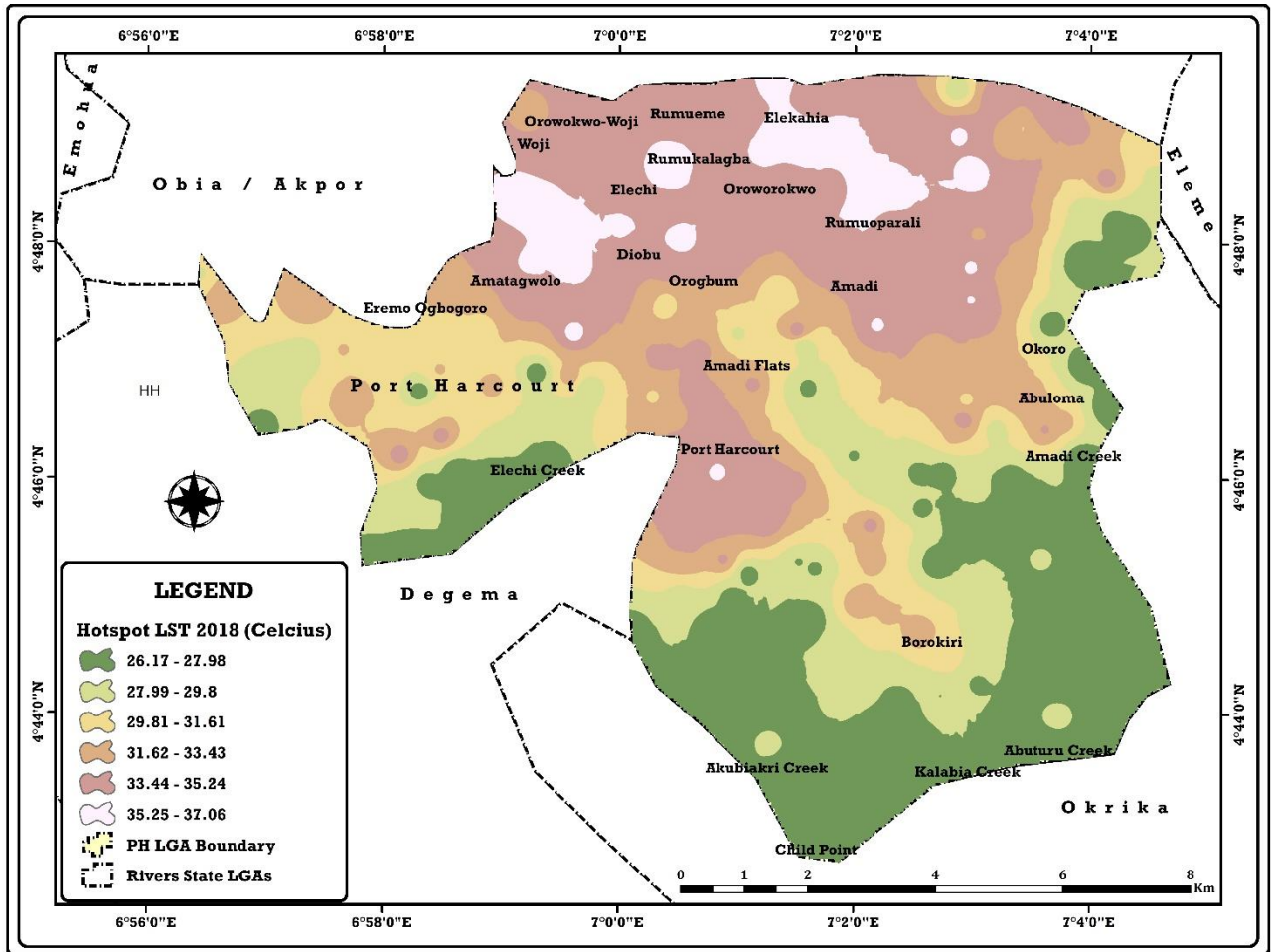


Figure 5.12: LST using Hotspots within Port Harcourt in 2018

These results demonstrate that the hotspots were in direct correspondence with the results of the land surface temperature analysis over Port Harcourt from 1986 to 2018. The presence of an urban heat island is currently established, as a distinct monotonous spatial relationship is observed between the hot spots who occupy the northern/central regions more readily, and the cold spots who are predominant in the southern regions and parts of the west.

### 5.5 Recommendations

In the light of the results of this research, it goes without saying that a problem identified only becomes a reference point when efforts are made to resolve and asphyxiate its impact. This research will therefore not be complete without an attempt at proffering solutions and making recommendations of importance to urban climate issues felt in the FCC. [17] suggests that it is possible to improve urban climate through urban planning and design, city planning should be given great attention in the tropics. The following been discussed briefly are also recommended to minimize the future occurrences of urban heat island's in the study area;

1. The introduction of building materials that will increase the albedos in the living areas. A low albedo value, characteristics of black asphalt absorb a large percentage of solar heat creating warmer near surface temperature. This can be achieved by using light coloured concrete which has high reflective appearance and reducing ambient temperature. Also, neighbourhoods may be able to lower average temperatures if they pave with light coloured concrete replacing the asphalt concrete
2. Another option suggested is to increase the amount of well-watered vegetation. This refers to adoption of “green roofs” (GR). Green roofs are known to be excellent insulators during the warm weather month in which the plants cool the surrounding environment. Air quality is empowered as the plant absorbs and converts carbon dioxide (CO<sup>2</sup>) to oxygen.
3. It has been observed that rapid temperature changes can be stressful to aquatic ecosystems. Therefore, this study recommends the construction of permeable pavements in the residential areas through which the effects of percolating water are paved into surface storage areas where it can be dissipated through absorption and evaporation.
4. The Green Building Programs Initiative (GBPI) should also be adopted as a measure a decrease buildings energy production and reduce the heat island effect .i.e. encouraging site with roof coverage from vegetation, highly reflective materials or a combination of the two.
5. Future factors like urban geometrics should be addressed by urban planners, architect and builders etc. The height and spacing of buildings affect the amount radiation received and emitted by urban infrastructures.
6. City planning; location of the cities in a region, its layout and orientation, street network, density of built up area, types of buildings and green area should be carefully planned.
7. Plants should be introduced to building in their roofs, facades and surrounding to provide thermal comfort. This is also called roof top gardening; wall climbing plants should be planted too. In Europe and America where temperatures are not even as high, this is a very common practice. Nigerian architecture can learn to be inclusive of that to help maintain a relatively cool micro-climate through all seasons.
8. The use of traditional building materials even in our cities such as timber and bamboo should be promoted. This can help alleviate the effects from the sun, the advantages are that they are light weight, have low thermal capacity which reduces solar heating accumulation during day time and long wave heat release at night. Thatch can be used for roofing since it is commonly found, cheap and durable, it also helps cool the buildings. These among others are some of the reasons why rural areas are proven to be always cooler than the cities.

## **6. Conclusion**

In this research, qualitative and quantitative analyses have been used to study the relationship between LULC and LST as an indicator for Urban Heat Island (UHI) occurrence over Port Harcourt L.G.A, Rivers State, Nigeria. The following conclusions were made: (1) Vegetative land cover has decreased rapidly from 1986 (2) Urban areas have increased in the study area and contributed to the variations in the spatial and temporal LST and affected the UHI intensity primarily through suburban sprawl, soil impaction and deforestation. (3) Hotspots are persistent in certain towns within the study area, while the cold spots vary more.

## References

- [1]. Adebayo, F. F., Balogun, I., Adediji, A., Olumide, A., & Abdulkareem, S. (2017). Assessment of Urban Heat Island over Ibadan Metropolis Using LANDSAT and MODIS. *International Journal of Environment and Bioenergy*, 10(8), 62-87.
- [2]. Adinna, E. N., Enete, I., & Okolie, T. (2009, February). Assessment of urban heat island and possible adaptations in Enugu urban using landsat-ETM. *Journal of Geography and Regional Planning*, 2(2), 030-036.
- [3]. Anderson, James R., Hardy, Ernest E., and Roach, John T., 1972, A land-use classification system for use with remote-sensor data: U.S. Geol. Survey Circ. 671, 16 p., refs.
- [4]. Ayoade, J.O. (1993) Urban Climate Studies in Tropical Africa: Problems and Prospects. The First International Conference of the African Meteorological Society, Nairobi, 8-12 February 1993, 7-11
- [5]. Chen, X., Zhao, H., Lia, P., & Yin, Z. (2006). Remote Sensing Image-Based Analysis of the Relationship Between Urban Heat Island and Land Use/Cover Changes. *Remote Sensing of Environment*, 104(34), 133-146. Retrieved August 2017
- [6]. Chow, W. T., & Roth, M. (2006). Temporal Dynamics Of The Urban Heat Island Of Singapore. *International Journal Of Climatology*, 8(5), 2243–2260.
- [7]. Enete, I. C., & Okwu, V. U. (2013). Mapping Enugu City’s Urban Heat Island. *International Journal of Environmental Protection and Policy*, 1(4), 50-58. doi:10.11648/j.ijepp.20130104.12
- [8]. Enete, I., & Alabi, M. O. (2012). Characteristics Of Urban Heat Island In Enugu During Rainy Season. *Ethiopian Journal of Environmental Studies and Management*, 8(4), 391-393.
- [9]. Enete, I., Awuh, M., & Ikekeazu, F. (2014). Assessment of Urban Heat Island (Uhi) Situation in Douala, Cameroon. *Journal of Geography and Earth Sciences*, 2(6), 55-77.
- [10]. Fujibe, F. (2009). Detection of Urban Warming in Recent Temperature Trends in Japan. *International Journal of Climatology*, 29(12) pp 1811-1822. DOI: 10.1002/joc.1822.
- [11]. Ifatimehin, O. O. (2007). An Assessment of Urban Heat Island of Lokoja Town Using LANDSAT ETM data. *International Journal of Ecology and Environmental Dynamics*, 24(4), 1-13.
- [12]. Inyang, E., Unung, O., & Ekanem, J. (2013). Evaluation of exposures to extremes of climate variability among rain-fed dependent vegetable farmers in a Niger-delta region, Nigeria. *African Journal of Agriculture, Technology and Environment (AJATE)*. 2(2):56-65
- [13]. Lehmann, S. (2010). Green urbanism: Formulating a series of holistic principles. *Sapiens*, 3(2).
- [14]. Li, Y., Zhang, H., & Kainz, W. (2012). Monitoring patterns of urban heat islands of the fast-growing Shanghai metropolis China: Using time-series of Landsat TM/ETM+data. *International Journal of Applied Earth Observation and Geoinformation*(19), 127-138.
- [15]. Okoye, T.O. (1975): “Port-Harcourt” in Ofomata, G. E. K. (ed). *Nigeria in maps: Eastern States*. Ethiope, Benin City. Pp. 92-93
- [16]. Lin, L., & Yuanzhi, Z. (2011). Urban Heat Island Analysis Using the Landsat TM Data and ASTER Data: A Case Study in Hong Kong. *International Journal of Remote Sensing*, 1535-1552.
- [17]. Roth, M. (2013). Urban Heat Islands. (H. Joseph, & S. Fernando, Eds.) *Handbook of Environmental Fluid Dynamics*, II, 143-144. Retrieved October 2017

- [18]. Stehman, S. V. (1995), Thematic map accuracy assessment from the perspective of finite population sampling. *Int. J. Remote Sens.* 16:589–593
- [19]. Streuker, D. R. (2012). A Remote Sensing Study of The Urban Heat Island of Houston. *International Journal of Remote Sensing*, 22(13): 2595-2608.
- [20]. Ujoh, F., Kwabe, J., & Ifatimehin, O. (2010). Understanding Urban Sprawl in the Federal Capital City, Abuja: Towards Sustainable Urbanization in Nigeria. *Journal of Geography and Regional Planning*, Vol. 35, pp 106 – 113.
- [21]. Umeuduji J.E., Aisuebeogun A., 1999. Relief and drainage in Port Harcourt Region. In: C.U.Oyegun, A.Adeyemo (eds), *A Paragraphics*, Port Harcourt
- [22]. Wang, G., Jiang, W., & Wei, M. (2008). An Assessment of Urban Heat Island Effect using Remote Sensing Data. *Marine Science Bulletin*, 14-25.
- [23]. Wong, N. H., & Chen, Y. (2009). *Tropical Urban Heat Islands: Climate, Buildings And Greenery*. London: Taylor and Francis.